Resonance Raman Investigation of the Interaction of Thromboxane Synthase with Substrate Analogues†

Zhucheng Chen,‡ Lee-Ho Wang,§ and Johannes P. M. Schelvis*,‡

Department of Chemistry, New York University, 31 Washington Place, Room 1001, New York, New York 10003, and Division of Hematology, Department of Internal Medicine, University of Texas Medical School, 6431 Fannin, Houston, Texas 77030

Received November 20, 2002; Revised Manuscript Received January 15, 2003

ABSTRACT: Thromboxane synthase is a hemethiolate enzyme that catalyzes the isomerization of prostaglandin H_2 to thromboxane A_2. We report the first resonance Raman (RR) spectra of recombinant human thromboxane synthase (TXAS) in both the presence and the absence of substrate analogues U44069 and U46619. The resting enzyme and its U44069 complex are found to have a 6-coordinate, low spin (6c/ls) heme, in agreement with earlier experiments. The U46619-bound enzyme is detected as a 6c/ls heme too, which is in contradiction with a previous conclusion based on absorption difference spectroscopy. Two new vibrations at 368 and 424 cm^{-1} are observed upon binding of the substrate analogues in the heme pocket and are assigned to the second propionate and vinyl bending modes, respectively. We interpret the changes in these vibrational modes as the disruption of the protein environment and the hydrogen-bonding network of one of the propionate groups when the substrate analogues enter the heme pocket. We use carbocyclic thromboxane A_2 (CTA_2) to convert the TXAS heme cofactor to its 5-coordinate, high spin (5c/hs) form, as is confirmed by optical and RR spectroscopy. In this 5c/hs state of the enzyme, the Fe−S stretching frequency is determined at 350 cm^{-1} with excitation at 356.4 nm. This assignment is supported by comparison to the spectrum of resting enzyme excited at 356.4 nm and by exciting at different wavelengths. Implications of our findings for substrate binding and the catalytic mechanism of TXAS will be discussed.

Thromboxane synthase (TXAS)[1] catalyzes the isomerization of prostaglandin H_2 (PGH_2) to thromboxane A_2 (TXA_2), a potent inducer of vasoconstriction and platelet aggregation (*1*−*3*). TXA_2 is believed to be a crucial physiological factor contributing to a variety of cardiovascular and pulmonary diseases such as atherosclerosis, myocardial infraction, and primary pulmonary hypertension. Therefore, studies on this enzyme are not only of chemical interest but also of pharmacological importance. TXAS has been isolated from human platelets and characterized as a cytochrome P450 (P450) enzyme by Ullrich and co-workers, and this assignment has been confirmed by its cDNA sequence (*4*, *5*). The heme iron in TXAS is known to be ferric 6c/ls with a cysteine thiolate as its proximal ligand, and the distal ligand is probably a water molecule (*4*, *6*). TXAS is a nontypical P450 enzyme. The typical P450 hydroxylation reaction requires molecular oxygen and a reductase to transfer electrons from NAD(P)H to the heme cofactor, but TXAS catalyzes the isomerization of PGH_2 without the need for molecular oxygen or any external electron donor (*7*−*9*). Besides TXA_2, malondialdehyde (MDA) and hydroxyheptadeca-trienoic acid (HHT) are formed in equimolar amounts (*4*). Since the reaction of TXAS with PGH_2 is very fast, substrate analogues (U44069 and U46619) are widely used to mimic the binding of substrate into the heme pocket of TXAS. In U44069, O(11) of the substrate is replaced by a carbon atom, while O(9) is substituted in U46619, as shown in Figure 1. On the basis of optical studies with substrate analogues and reactions with isotopically labeled PGH_2, a mechanistic model has been proposed for TXAS involving specific binding of PGH_2 to the heme iron with its O(9), while it has been suggested that it cannot coordinate to the heme iron with its O(11), leading to a 5c/hs species when U46619 is used. Furthermore, the proposed mechanism predicts the homolytic cleavage of the endoperoxide bond resulting in the formation of a reaction intermediate with its O(9) bound to the heme iron (*8*, *9*). EPR data have corroborated the formation of a 6c/ls heme with U44069, but not much spectroscopic data is available to provide evidence for the binding model of U46619, and little is known on how the protein environment (e.g., the proximal ligand) contributes to substrate binding and the catalytic mechanism. Recently, Wang and co-workers successfully overexpressed human TXAS in *Escherichia coli*, which has the same properties as the platelet enzyme (*6*). The large amount of TXAS that is now available from the bacterial

† This work was supported by start-up funds from New York University (J.P.M S.) and by Grant HL-60625 from the National Institutes of Health (L.-H.W.).

* To whom correspondence should be addressed. Tel: (212) 998-3597. Fax: (212) 260-7905. E-mail: hans.schelvis@nyu.edu.

‡ New York University.

§ University of Texas Medical School.

[1] Abbreviations: LS, 6C, low spin, 6-coordinate; HS, 5C, high spin, 5-coordinate; RR, resonance Raman; Mb, myoglobin; Hb, hemoglobin; TXAS, thromboxane synthase; P450, cytochrome P450; CPO, chloroperoxidase; NOS, nitric oxide synthase; CBS, cystathionine β-synthase; IDO, indoleamine 2,3-dixoygenase; Cyt *c*, cytochrome *c*; KatG, *Mycobacterium tuberculosis* catalase-peroxidase; MDA, malondialdehyde; HHT, hydroxylheptadecatrienoic acid.

10.1021/bi027206s CCC: $25.00
Published on Web 02/12/2003

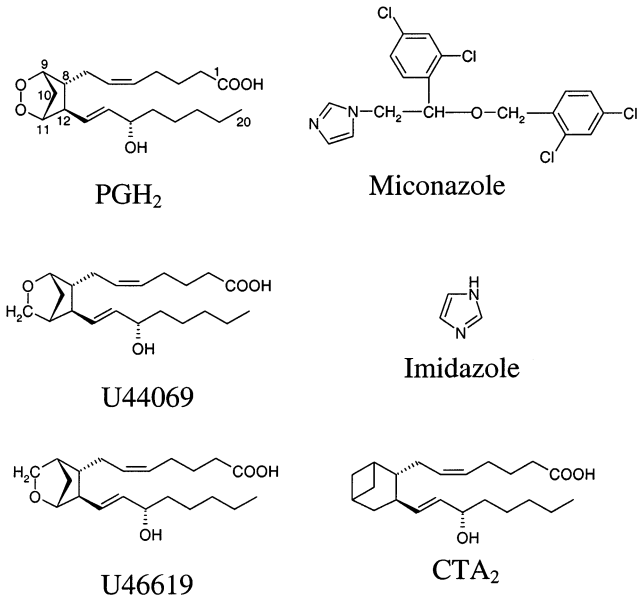

FIGURE 1: Structure of the TXAS substrate prostaglandin H_2 (PGH_2) and of two substrate analogues, U44069 and U46619. The structures of three other ligands used in this study are also shown (i.e., miconazole, imidazole, and carbocyclic thromboxane A_2 (CTA_2)).

expression system makes the enzyme suitable for detailed spectroscopic investigations.

In this paper, we use resonance Raman spectroscopy to investigate the TXAS heme, its protein environment, and its interaction with substrate analogues. Resonance Raman (RR) spectroscopy is a powerful tool to explore the heme environment and the iron spin and coordination states, making it ideal for studies of substrate interaction and reaction mechanisms in hemoproteins in aqueous solution. In addition, the quantitative measurement of the Fe−S vibrational frequency (νFe−S) can be used as an assessment of the strength of Fe−S bond, which is proposed to be critically involved in the formation of the reaction intermediates (*10*, *11*). Extensive work of RR spectroscopy has been done on hemethiolate enzymes P450 (*12*, *13*), chloroperoxidase [CPO] (*14*, *15*), cystathionine β-synthase [CBS] (*16*), and nitric oxide synthase [NOS] (*17*−*20*). On the basis of RR studies of resting and substrate-analogue bound TXAS, we propose that both the O(11) and the O(9) of PGH_2 can coordinate to the heme iron of TXAS, which is in contradiction with a previous conclusion. Furthermore, we find evidence for disruption of the hydrogen-bonding network of a propionate group on substrate binding. The Fe−S stretching frequency is determined to be similar to that of P450 and CPO. The implications of our findings for the TXAS reaction mechanism will be discussed.

EXPERIMENTAL METHODS

Materials. Substrate analogues, U44069 and U46619, and CTA_2 were purchased from Cayman Chemical Company. In the case of CTA_2, solvent (ethanol) was evaporated before adding CTA_2 to the sample in the experiment excited with 356.4 nm laser light. All other chemicals were purchased from Sigma-Aldrich.

Enzyme Preparation. TXAS was obtained from a bacterial expression system as previously described (*6*). The first 28 amino acid residues of the N-terminus have been deleted and replaced with MALLLAVF to enhance the expression level, and four histidine residues have been added at the C-terminus to facilitate purification. The enzyme was stored at a final concentration of 24 μM in a pH 7.5 phosphate buffer solution containing 0.2% Emulgen 913 and 10% glycerol. The recombinant TXAS exhibits similar UV−vis and EPR properties as the native platelet TXAS and has also similar K_m and V_{max} values as TXAS isolated from platelets with regard to the TXA_2 and MDA formation (*6*, *21*).

Electronic Absorption Spectroscopy. Electronic absorption spectra were obtained at room temperature with a UV−vis spectrophotometer (Lambda P40, Perkin-Elmer) with the sample sealed in a Raman spinning cell. Absorption spectra of all samples were taken before and after the resonance Raman experiments to ensure sample integrity. CTA_2 titration was performed in a quartz cuvette with a 1 cm path length.

Resonance Raman Spectroscopy. Resonance Raman spectra were collected using a single spectrograph (TriAx 550, JY/Horiba) and a N_2(l)-cooled CCD detector (Spectrum One, JY/Horiba) with a UV-enhanced 2048 × 512 pixels chip (EEV) as described previously (*20*). Rayleigh scattering was removed from the Raman signal by using the appropiate holographic notch filters (Kaiser Optical). The samples were placed in a spinning cell under a N_2 atmosphere and kept at 7−10 °C during the experiments. The 356.4, 406.7, or 413.1 nm lines from a Kr^+ laser (Coherent, I-302) were used for the excitation of the sample. The laser power incident on the sample was 10 mW unless stated otherwise. The RR experiments had a marginal effect on the enzymatic activities, as TXAS retained 80−90% of its activity after laser irradiation. Details about the sample preparation are indicated in the figure legends. The resonance Raman spectra were corrected for a background by subtracting a polynomial function, and toluene was used to calibrate the RR spectra. Raman vibrations were labeled and assigned according to the literature (*22*−*24*).

RESULTS

UV−vis Absorption Spectra. Figure 2A shows the absorption spectra of the ferric form of TXAS and its ligand-bound complex. The Soret band maximum of the heme in TXAS occurs at 417 nm, and the binding of U44069 and U46619 in the heme pocket shifts the Soret band of the heme to 413 and 414 nm, respectively. This slight blue shift suggests that the enzyme remains 6c/ls. The absorption difference spectra are given in Figure 2B and are in good agreement with those reported by Ullrich et al. (*8*, *9*). In the case of U44069, the change in Soret absorption has been interpreted as the replacement of water by O(9) of U44069 as the sixth ligand (*6*, *8*). In the case of U46619-bound TXAS, a peak at 394 nm and a trough at 423 nm in the optical difference spectrum have been interpreted as the formation of a 5c/hs heme. Further results about the coordination state of the heme in the presence of the substrate analogues will be discussed in the RR section. Addition of imidazole and miconazole to the enzyme induces a red shift, indicating removal of the water molecule as the sixth ligand and nitrogen coordination to the heme iron (*6*, *25*).

RR Spectra of Resting TXAS and Its Ligand-Bound Complex. The high-frequency RR spectrum of TXAS is shown in Figure 3. The spectrum of the enzyme has main

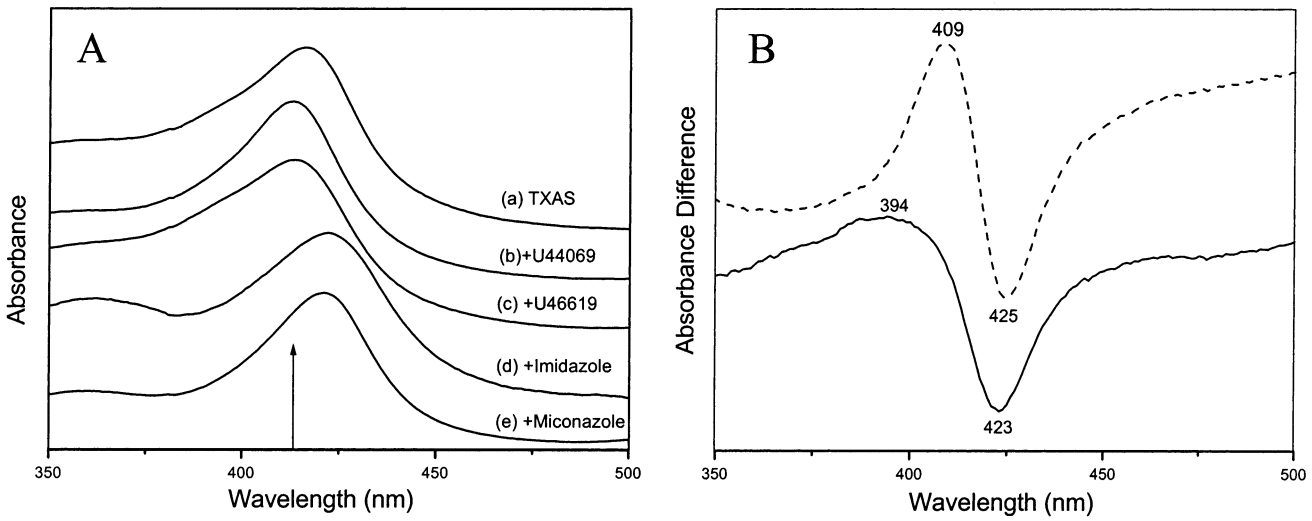

FIGURE 2: (A) Optical absorption spectra of resting and ligand-bound TXAS (24 μM). (a) Resting, (b) 0.47 mM U44069, (c) 0.9 mM U46619, (d) 1.0 mM imidazole, and (e) 0.1 mM miconazole. The vertical arrow indicates the excitation wavelength of the RR experiments at 413.1 nm. (B) Optical difference spectra of TXAS with substrate analogues U44069 (dashed line) and U46619 (solid line) at 300 μM ligand concentration.

vibrational peaks at 1374, 1503, 1564, 1587, and 1638 cm^{-1}. These peaks are assigned to the heme skeletal vibrations and indicate the oxidation, coordination, and spin state of the heme iron (*22*−*24*). The oxidation state marker band, ν_4, occurs at 1374 cm^{-1}. The core size marker bands, ν_3, ν_2, and ν_{10}, are sensitive to the spin state and coordination state of the heme iron. The peak at 1503 cm^{-1} is assigned to ν_3 vibration. The ν_2 region, 1550−1600 cm^{-1}, is usually crowded with other vibrations, such as ν_{11}, ν_{19}, and ν_{17}, which makes it difficult to assign the ν_2 vibration accurately. In this paper, we assign the peak at 1564 cm^{-1} to the ν_{11} vibration and the peak at 1587 cm^{-1} to the ν_2 vibration. The peak observed at 1638 cm^{-1} is assigned to the ν_{10} vibration, convoluted with two other peaks at 1621 and 1630 cm^{-1}, which are assigned to two vinyl stretching vibrations. These assignments are summarized in Table 1 together with those of other hemethiolate enzymes. The ν_4, ν_3, ν_{11}, ν_2, and ν_{10} vibrations at 1374, 1503, 1564, 1587, and 1638 cm^{-1}, respectively, are characteristic of a 6c/ls ferric heme, in agreement with our absorption spectrum and previous results (*6*, *8*).

Addition of the substrate analogues, U44069 and U46619, to the enzyme causes only small changes in the high-frequency RR spectra, as shown in Figure 3A, lines b and c. The ν_4, ν_3, ν_{11}, and ν_2 vibrations of the U44069-bound enzyme occur at almost the same frequencies as in the resting enzyme. The ν_{10} vibration at 1640 cm^{-1} is well-separated from the vinyl stretching vibrations. All the heme core marker bands indicate a 6c/ls state of the U44069-bound enzyme, in agreement with the previous absorption spectra and EPR results (*4*, *6*). The high-frequency RR spectrum obtained from U46619-bound enzyme, however, contradicts the result from the optical difference spectrum. The ν_4, ν_3, ν_{11}, ν_2, and ν_{10} vibrations of U46619-bound enzyme occur at 1374, 1503, 1564, 1587, and 1640 cm^{-1}, respectively, representing a 6c/ls form of the enzyme but was reported as 5c/hs based on optical difference spectra (*8*, *9*). To explore the potential assignment for a 5c/hs species further, we excited the U46619-bound enzyme with 406.7 and 356.4 nm laser light, which is expected to enhance the 5c/hs form of enzyme, if there is any, over the 6c/ls form. As shown in Figure 3B, the frequencies of the ν_4, ν_3, ν_2, and ν_{10} vibrations are 1373, 1503, 1587, and 1640 cm^{-1}, respectively, in the spectra obtained with excitation at these wavelengths. These results indicate no detectable 5c/hs species but only 6c/ls heme. Despite the fact that we obtain the same absorption difference spectrum as reported earlier (*8*, *9*), our RR data argue strongly against a 5c/hs heme and favor a 6c/ls heme when U46619 binds to TXAS.

The absorption spectrum of TXAS + U46619 was obtained at 25 °C, while the RR spectra were acquired at 7−10 °C. Since the conversion between hs and ls is temperature dependent (*26*), we measured the high-frequency RR spectra of the U46619-bound enzyme at room temperature (25 °C), as shown in Figure 3C. When excited at 406.7 nm with a power of 1.5 mW, the main vibrations occurred at 1373, 1503, 1564, 1587, and 1640 cm^{-1}, which are assigned to the ν_4, ν_3, ν_{11}, ν_2, and ν_{10} vibrations, respectively, indicating a 6c/ls heme. A weak vibration at 1487 cm^{-1} was also detected, which may be assigned to the ν_3 vibration of a 5c/hs heme. This weak vibration of 5c/hs heme may be due to photolysis of the protein at room temperature under exposure to laser light, as its intensity increases slightly when 10 mW laser power was used, Figure 3C. The RR spectra obtained at room temperature predominantly show the vibrations of a 6c/ls heme and rule out the possibility that the temperature changes the spin state of the enzyme between 7 and 25 °C. The optical difference spectrum obtained at 7 °C is also similar to the one obtained at 25 °C (data not shown).

In the low-frequency region, Figure 4, the assigned heme skeletal modes in TXAS are ν_7 (675 cm^{-1}), ν_{15} (754 cm^{-1}), and ν_8 (340 cm^{-1}). On the basis of the complete assignment of met-myoglobin (metMb), deoxy Mb, and cytochrome *c* (Cyt *c*), the vibration observed at 378 cm^{-1} is assigned to the bending modes, δ ($C_\beta C_c C_d$)$_{6,7}$, of the heme propionate groups, and the peak at 408 cm^{-1} and its shoulder at 424 cm^{-1} are assigned to two bending modes, δ ($C_\beta C_a C_c$)$_{2,4}$, of the vinyl groups (*27*, *28*). These assignments are summarized together with those of other heme proteins in Table 2.

The low-frequency vibrational modes are not as sensitive to the spin and coordination state of the heme, but they can

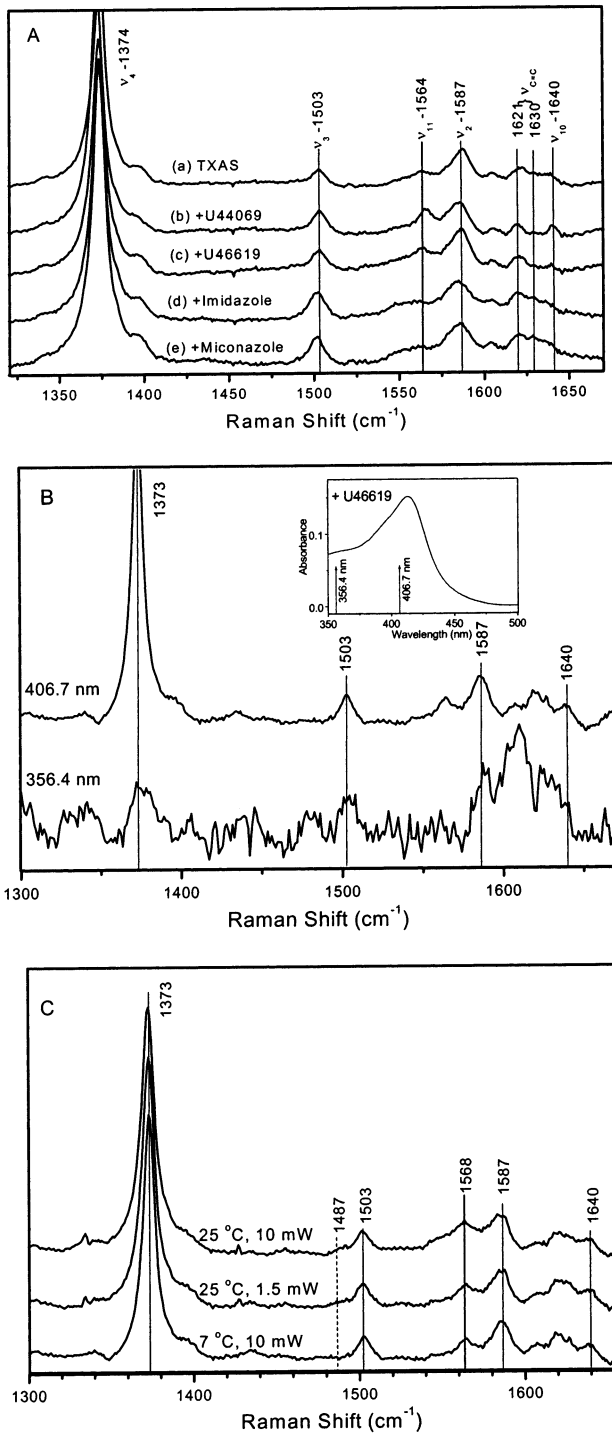

FIGURE 3: High-frequency RR spectra of various forms of TXAS (A) excited at 413.1 nm. (a) Resting, (b) U44069-bound, (c) U46619-bound, (d) imidazole-bound, and (e) miconazole-bound enzyme. The spectrum of the buffer was subtracted to remove the contributions of glycerol. The enzyme and ligand concentrations are the same as described in Figure 2A. (B) U46619-bound enzyme excited at 406.7 and 356.4 nm. Insert: Absorption spectrum of U46619-bound TXAS and the position of the excitation wavelengths. (C) U46619-bound enzyme excited at 406.7 nm at 7 and 25 °C and with different laser power, 1.5 and 10 mW.

provide information about the interaction between the heme cofactor and its protein environment. The binding of substrate analogues does not induce a significant change in the heme skeletal vibrations, ν_8, ν_7, and ν_{15}, in the low-frequency region, as shown in Figure 4, lines b and c, in agreement

Table 1: Observed Heme Skeletal and Fe−S Vibrations of TXAS and Other P450-Like Hemoproteins in cm^{-1}

	ν_4	ν_3	ν_2	ν_{10}	ν(Fe−S)	assign-ment	ref
TXAS	1374	1503	1587	1638		LS,6C	this paper
TXAS-U44069	1373	1503	1586	1640		LS,6C	this paper
TXAS-U46619	1374	1503	1587	1640		LS,6C	this paper
TXAS-Im	1374	1502	1585	1637		LS,6C	this paper
TXAS-miconazole	1374	1502	1586	1637		LS,6C	this paper
P450	1373	1503	1584	1631		LS,6C	13
eNOS	1374	1503	1579	1635		LS,6C	20
CPO	1373	1504	nd[b]	1638		LS,6C	14
TXAS-CTA$_2$	1373	1503	1586	1638	350	LS,6C	this paper
	1371	1487	1568			HS,5C	
P450[a]	1368	1488	1570	1623	351	HS,5C	12,13
eNOS[a]	1370	1489	1563	nd[b]	338	HS,5C	20
CPO	1369	1490	1567	nd[b]	347	HS,5C	15
CBS	1372	1500	1575	1630	312	LS,6C	16

[a] Substrate bound form. [b] nd: not detected.

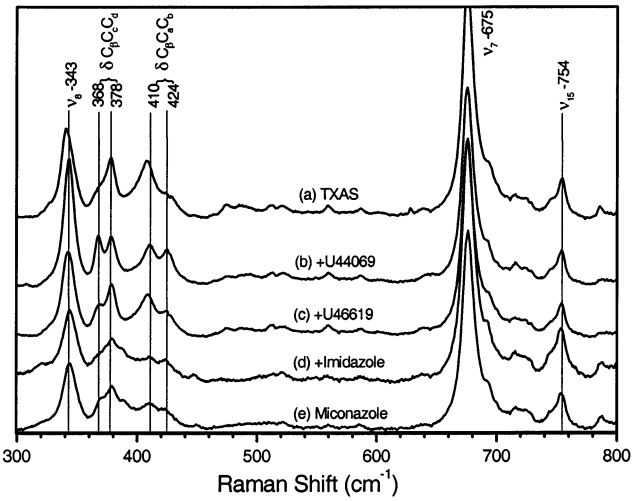

FIGURE 4: Low-frequency RR spectra of various forms of TXAS excited at 413.1 nm. (a) Resting, (b) U44069-bound, (c) U46619-bound, (d) imidazole-bound, and (e) miconazole-bound. The concentrations are the same as described in Figure 2A.

Table 2: Observed Low-Frequency Modes of TXAS and Other Hemoproteins in cm^{-1}

	ν_8	$\delta(C_\beta C_c C_d)$	$\delta(C_\beta C_a C_b)$	ν_7	ν_{15}	ref
TXAS	340	378	408, 424[a]	675	754	this paper
TXAS-U44069	343	378,368	410, 424	675	754	this paper
TXAS-U46619	342	378,368	409, 424	675	754	this paper
TXAS-Im	344	379	410, 424	675	754	this paper
TXAS-miconazole	344	379,369	410, 424	675	753	this paper
TXAS-CTA$_2$	344	378	408, 424	677	754	this paper
P450	347	379	424	678	753	13
MetMb	344	376	409, 440	674	757	27
deoxyMb	342	370	405, 436	672	756	27
ferrocyt C	347	382,372	413, 421	700	750	28
Hb M Iwate	343	381,370	411,426	nr[b]	nr[b]	30

[a] A shoulder peak. [b] nr: not reported.

with the high-frequency spectra. However, the introduction of substrate analogues causes dramatic changes in the bending modes of both vinyl and propionate groups, δ ($C_\beta C_a$ C_b) and δ ($C_\beta C_c$ C_d), respectively. The new vibration at 368 cm^{-1} is attributed to a lower frequency bending mode of the propionate groups. Another bending mode of the propionate groups is observed at the same position as in the resting enzyme (378 cm^{-1}) but has lost intensity. Two bending modes of the vinyl groups are detected. The higher

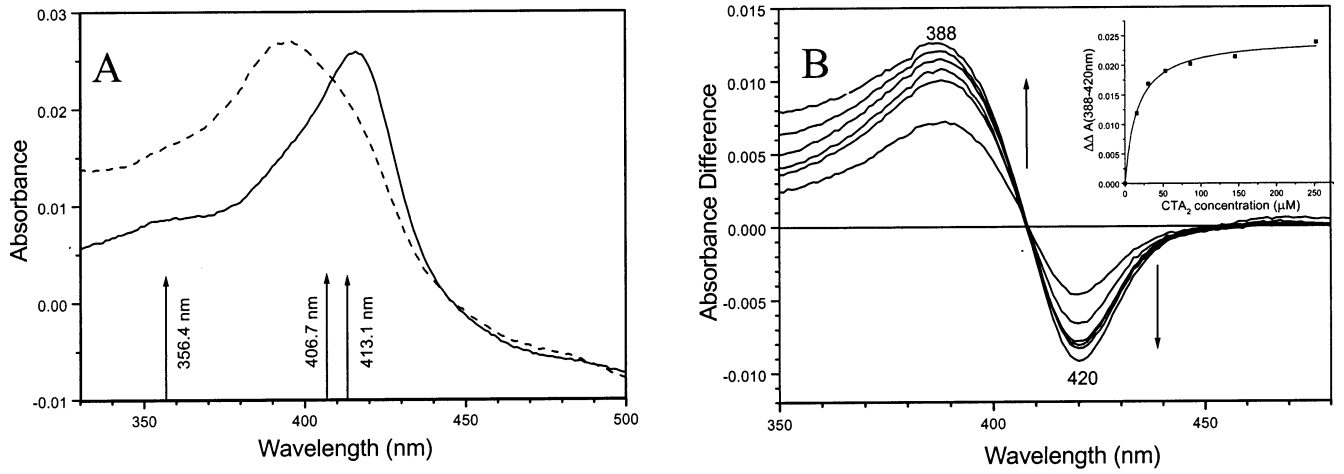

FIGURE 5: (A) Optical absorption spectra for resting (solid line) and CTA_2 bound (dashed line) TXAS. The concentration of CTA_2 in the sample is 0.25 mM. The vertical arrows indicate the excitation wavelengths at which RR spectra were collected. (B) Titration of TXAS with CTA_2. The optical difference spectra correspond to the following increasing ligand concentrations: 16, 30, 54, 86, 146, and 253 μM. The arrows indicate the directions of the changes. The inset panel shows the titration curve with one-site-binding curve fit giving a dissociation constant, K_d, of 16 μM.

frequency mode at 424 cm^{-1} is enhanced on introducing the substrate analogues into the heme pocket, while the intensity of the lower frequency mode at 410 cm^{-1} decreases. The vibrations of both propionate groups and vinyl groups are believed to be sensitive to the protein environment around the heme cofactor (*29*−*39*). For either substituent group of the heme in TXAS, the activation of one bending mode at the expense of the other demonstrates that the binding of substrate analogues in the heme pocket changes the interaction between the heme and the protein matrix.

To explore these disruption effects induced by the distal ligands in more detail, we used a small molecule, imidazole, and a large one, miconazole, as probes of the distal cavity of the heme pocket. The high-frequency RR spectra of TXAS in the presence of imidazole and miconazole are shown in Figure 3A, lines d and e, respectively, and indicate 6c/ls hemes. Two vinyl stretching modes can be observed at 1621 and 1630 cm^{-1}. In the low-frequency region (Figure 4, lines d and e), both of these ligands can enhance the vinyl bending mode at 424 cm^{-1}, as observed in the substrate analogue-bound enzyme. However, they induce a different response from the propionate groups. In the imidazole-bound enzyme, only the higher propionate bending frequency (379 cm^{-1}) can be detected, while for the miconazole-bound enzyme, not only the higher frequency mode (379 cm^{-1}) but also the lower frequency mode at 368 cm^{-1} is observed with a reduced intensity similar to U46619. These results support our proposal that large distal ligands can interact with one of the heme propionate groups in TXAS.

Detection of the Fe−*S Vibration.* To this date, most of the Fe−S vibrations in P450 super-family enzymes have been detected for the 5c/hs heme state (*12*, *15*, *20*). To produce such a 5c/hs form of TXAS, carbocyclic thromboxane A_2 (CTA_2) was selected from various candidates and found to be a valuable compound to produce 5c/hs heme in TXAS. UV−vis absorption spectra of the free and CTA_2-bound enzyme are shown in Figure 5. The TXAS absorption spectrum shows a 22 nm blue shift of the Soret band on binding of CTA_2 in the heme pocket. This change suggests the expulsion of the distal ligand, presumably, a water molecule, and the change from a 6c/ls to a 5c/hs heme state. The absorption difference spectra at increasing CTA_2 concentration are shown in Figure 5B. As the concentration of CTA_2 increases, the absorption at 420 nm decreases and that at 388 nm increases monotonically. The corresponding titration curve is illustrated in the inset of Figure 5B. A fit of these data to a one-site-binding curve gives a dissociation constant, K_d, of 16 ± 2 μM, which is surprisingly close to that of U44069. This absorption difference spectrum is quite different from that of TXAS with U46619 bound (Figure 2B), which presumably produces a 5c/hs heme (*8*, *9*).

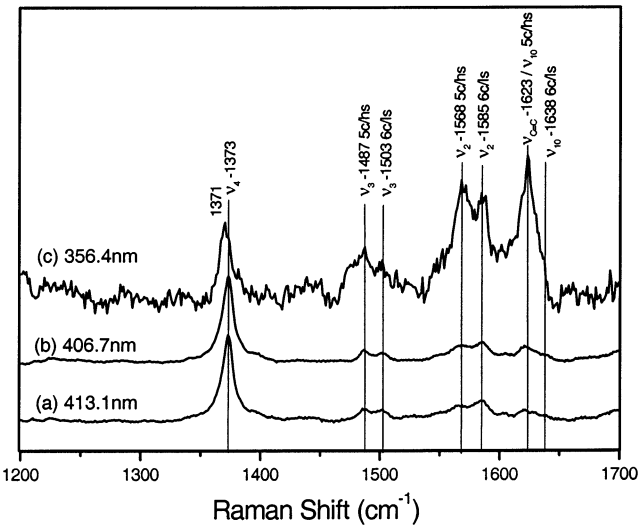

FIGURE 6: High-frequency RR spectra of CTA_2-bound TXAS excited at different wavelengths (λ_{ex}): (a) λ_{ex} = 413.1 nm, (b) λ_{ex} = 406.7 nm, and (c) λ_{ex} = 356.4 nm. Concentration of CTA_2 in the sample is 0.14 mM. The spectrum excited with 356.4 nm was collected for 1 h with a power of 15 mW.

High-frequency RR spectra of CTA_2-bound enzyme excited at different wavelengths are shown in Figure 6. The spectrum of CTA_2-bound enzyme excited with 413.1 nm in Figure 6, line a shows an about even contribution of vibrations of 6c/ls and 5c/hs hemes. The peak at 1373 cm^{-1} is assigned to the ν_4 vibration. The peaks at 1487 and 1503 cm^{-1} are assigned to ν_3 vibrations, and the peaks at 1568

and 1586 cm^{-1} are assigned to ν_2 vibrations. A shoulder peak at 1638 cm^{-1} is assigned to the ν_{10} vibration. The observation of two ν_3 and ν_2 vibrations indicates that the heme of CTA_2-bound enzyme is a mixture of 5c/hs and 6c/ls state. On the basis of the K_d measured above and the concentration of CTA_2, 90% of the enzyme should be converted to the 5c/hs heme state. The ν_4, ν_3, ν_2, and ν_{10} vibrations at 1373, 1503, 1586, and 1638 cm^{-1}, respectively, demonstrate the existence of 6c/ls ferric heme, while the ν_3 and ν_2 vibrations at 1487 and 1568 cm^{-1} indicate the presence of a 5c/hs ferric heme. The ν_4 and ν_{10} vibrations of the 5c/hs species are overlapped with the ν_4 vibration of the 6c/ls ferric heme and the vinyl stretching modes, respectively. The presence of a mixture of 5c/hs and 6c/ls heme states for the CTA_2-bound enzyme is supported by the RR spectra excited with 406.7 nm, which enhances the vibrations of the 5c/hs species. Two ν_3 (1487 and 1503 cm^{-1}) and ν_2 (1568 and 1586 cm^{-1}) vibrations can be observed. The vibrational modes corresponding to the 5c/hs state (i.e., ν_3 at 1487 cm^{-1} and ν_2 at 1568 cm^{-1}) have become more enhanced and confirm the presence of 5c/hs species in the CTA_2-bound enzyme.

When 356.4 nm excitation is used, the vibrations of 5c/hs species are more characteristic. The high-frequency RR spectra of CTA_2 bound TXAS is shown in Figure 6, line c. Exciting the heme molecules with UV light enhances nontotally symmetric vibrations. Totally symmetric vibrations such as ν_4, ν_3, and ν_2 are observed with lower intensity under this condition. The ν_4 vibration is detected at 1371 cm^{-1}, with a shoulder at 1373 cm^{-1}. The downshift of the ν_4 vibration when exciting with near-UV light is also observed in the cases of substrate bound P450 and NOS (*13*, *20*). The ν_3 and ν_2 vibrations of both 5c/hs and 6c/ls heme species are observed at the same frequencies as with visible light excitation. The vibrations representative of the 5c/hs heme state are stronger than those of the 6c/ls heme. The strong peak at 1623 cm^{-1} cannot be assigned at this moment because this region is crowded with the stretching modes of the vinyl groups and the ν_{10} vibration of 5c/hs heme. The multiple excitation wavelength experiments clearly indicate the presence of a 5c/hs heme in the CTA_2-bound enzyme.

Low-frequency RR spectra of CTA_2-bound enzyme excited at different wavelengths are shown in Figure 7. The spectra of CTA_2-bound enzyme excited at 413.1 and 406.7 nm (Figure 7, lines a and b) are similar to that of the resting enzyme since the low-frequency vibrations are not very sensitive to the coordination and spin state of the heme. The vibrations at 677 and 344 cm^{-1} are assigned to ν_7 and ν_8 modes, respectively. The peak at 754 cm^{-1} is assigned to the ν_{15} vibration, while the peak at 378 cm^{-1} is the bending mode of the propionate groups. Two bending modes of vinyl groups are observed at 408 and 424 cm^{-1}.

The Fe−S vibration in P450 and NOS were observed in 5c/hs enzyme excited with UV light, which excites the Fe−S charge transfer band (*14*). The low frequency RR spectrum of 5c/hs TXAS excited at 356.4 nm is shown in Figure 7, line c. The intensities of the vibrations are greatly decreased at this wavelength because 356.4 nm is far away from the maximum of the Soret band at 395 nm. The ν_7 vibration can still be observed around 677 cm^{-1} with a shoulder at 682 cm^{-1}. The bending modes of the propionate and the vinyl groups are detected at 379 and 424 cm^{-1}, respectively. The ν_8 vibration was not observed with 356.4 nm excitation.

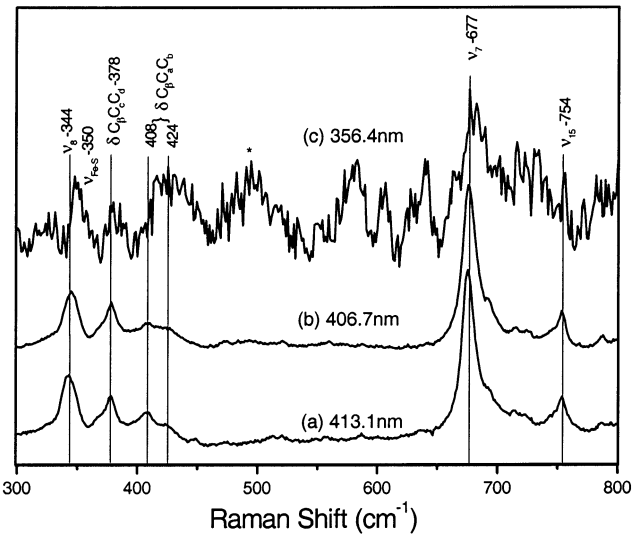

FIGURE 7: Low-frequency RR spectra of CTA_2-bound TXAS excited at different wavelengths (λ_{ex}): (a) λ_{ex} = 413.1 nm, (b) λ_{ex} = 406.7 nm, and (c) λ_{ex} = 356.4 nm. The conditions are the same as described in Figure 6. The asterisk indicates the quartz scattering from the sample cell.

Instead, a new vibration at 350 cm^{-1} is present, which is absent on excitation with 406.7 and 413.1 nm. These kinds of observations were also made for P450. In P450, the Fe−S vibration was measured at 351 cm^{-1}, while those in NOS and CPO were detected at 338 and 347 cm^{-1}, respectively, as summarized in Table 1. On the basis of these assignments, the new vibration at 350 cm^{-1} in CTA_2 bound TXAS is tentatively assigned to the Fe−S stretching vibration of 5c/hs ferric TXAS.

To clarify the assignment of 5c/hs TXAS excited at 356.4 nm, we can compare the spectra of substrate free and CTA_2-bound enzymes, as shown in Figure 8. Upon binding with CTA_2, the ν_4 vibration shifts from 1373 to 1371 cm^{-1}. Two new peaks, 1487 and 1568 cm^{-1}, appeared in the CTA_2-bound form of the enzyme, which are assigned to the ν_3 and ν_2 vibrations of 5c/hs species as mentioned above. The ν_{10} vibration at 1638 cm^{-1} has greatly lost its intensity when CTA_2 is bound. All of these results agree with the conversion of 6c/ls state heme into 5c/hs state and the enhancement of the later state with 356.4 nm excitation. In the low-frequency region, Figure 8B, the vibrations of free enzyme are similar to those of the CTA_2-bound enzyme, except in the region of 340−360 cm^{-1}. The lack of an obvious peak in this area for the resting enzyme rules out the possibility that the vibration of 350 cm^{-1} in the CTA_2-bound enzyme arises from the CTA_2-free enzyme and supports our assignment of this peak to the Fe−S stretching vibration.

DISCUSSION

Spin and Coordination States of Resting and Ligand-Bound TXAS. The high-frequency resonance Raman spectra shown in Figure 3, line a and the frequencies tabulated in Table 1, which compares TXAS to various other hemethiolate enzymes, indicate the presence of a 6c/ls ferric heme in TXAS, in agreement with previous absorption and EPR experiments.

The interaction of TXAS with substrate analogues U44069 and U46619 has been studied by Ullrich et al. using absorption difference and EPR spectroscopy. Our observation

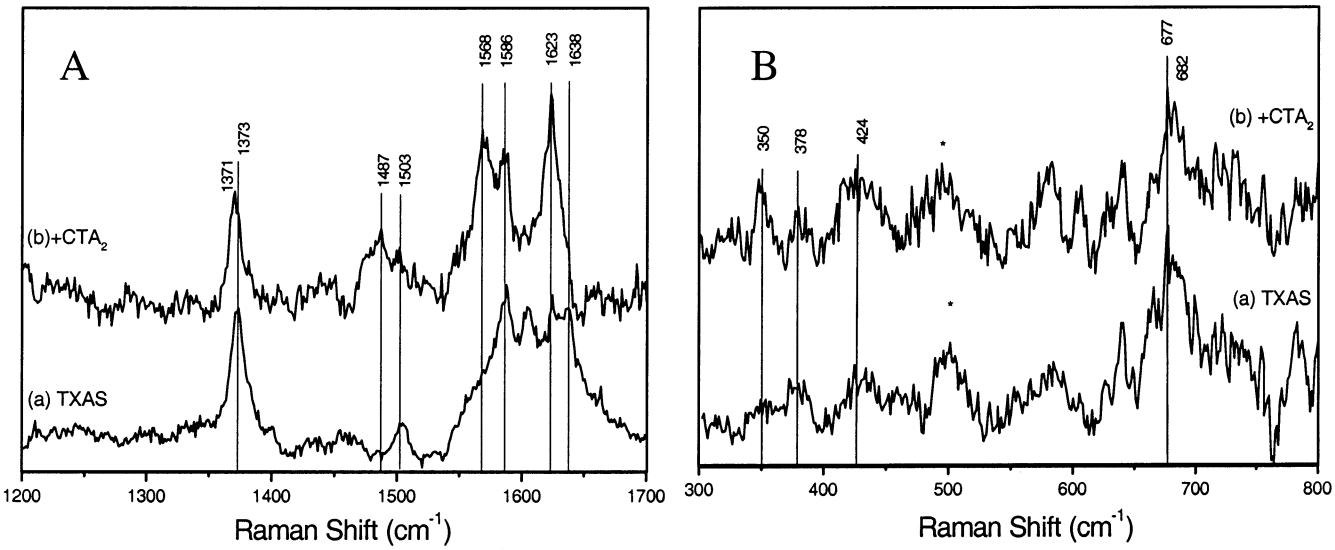

FIGURE 8: RR spectra of resting and CTA_2-bound TXAS excited at 356.4 nm. (A) High-frequency region and (B) low-frequency region. The conditions are the same as described in Figure 6. The asterisks indicate the quartz scattering from the sample cell.

of a 6c/ls heme in U44069-bound enzyme agrees well with earlier results (*6*, *8*). However, our result on U46619-bound enzyme is quite unexpected. In an earlier absorption difference spectroscopic study, it was proposed that the U46619-bound enzyme has a 5c/hs heme. In the present resonance Raman spectrum, all the core size marker bands, ν_3, ν_{11}, ν_2, and ν_{10}, which are sensitive to the spin and coordination state of the heme, indicate a 6c/ls heme instead of a 5c/hs heme. Even when excited at 406.7 and 356.4 nm, which can selectively enhance the vibrations of 5c/hs ferric heme, the enzyme still only shows a 6c/ls heme state. The vibrational features of the U46619-bound enzyme, Figure 3C, contrast sharply with those of CTA_2-bound enzyme, Figure 6. On the basis of the ν_3 vibration, 6c/ls heme is predominant with little or no 5c/hs heme in the U46619-bound enzyme, while 5c/hs heme is the major species in CTA_2-bound enzyme. Our RR spectrum of TXAS with U46619 indicates no obvious amount of high spin heme, except at 25 °C when a very small amount of 5c/hs may be observed, presumably, because of laser photolysis. The absolute absorption spectrum of U46619 bound enzyme is not characteristic of 5c/hs. Its Soret band is at 414 nm, as shown in Figure 2A, line c. Experiments on P450 showed a dramatic 30 nm-blue shift of the Soret band upon introduction of camphor into the heme pocket, in which the heme is known to change from 6c/ls to 5c/hs (*13*). In experiments of NOS, the Soret band shifts from 416 to 398 nm when its heme is converted from the 6c/ls to the 5c/hs state (*40*), and addition of CTA_2 to TXAS also produces a large shift in the Soret band from 417 to 395 nm. Compared to these known enzymes, the shift in the absolute absorption spectrum of TXAS on binding with U46619 is much smaller and may not be representative of changing from a 6s/ls to a 5c/hs heme. According to the RR spectra and absolute absorption spectra, we conclude that the heme present in U46619-bound TXAS is 6c/ls and that the observed difference spectrum cannot result from a 5c/hs heme but is due to other effects that remain to be investigated further.

Although large variations in the dissociation constants, K_d, measured for these substrate analogues have been reported, it is commonly believed that the affinity of TXAS for U44069 is higher than for U46619, indicating that the heme iron prefers to bind the O(9) rather than O(11) of the substrate (*6*, *8*, *41*, *42*). On the basis of this observation, an isomerization mechanism of PGH_2 has been proposed, in which binding of O(9) to the heme iron initiates a series of reactions, leading to the formation of TXA_2, while coordination of O(11) to the heme iron was not considered (*8*, *9*). The detection of a 6c/ls heme in both U44069 and U46619-bound enzyme suggests that both O(9) and O(11) endoperoxide atoms of the substrate can coordinate to the heme iron as the sixth ligand, although the latter one, presumably, coordinates by some flexibility of the ligand and/or the protein environment. More experiments are required to understand the selectivity of the enzyme to distinguish O(9) from O(11). By taking into account our new results, the reaction of TXAS with PGH_2 maybe more complicated than was proposed before. A side reaction when O(11) coordinates to the heme, potentially resulting in inhibition of the enzyme, or perhaps, formation of MDA and HHT, cannot be ruled out.

Protein Environment Around the Heme Cofactor. The two propionate and vinyl groups at the periphery of the heme cofactor can interact with the protein matrix. Various ligands introduced into the heme pocket can serve as probes to perturb such interactions.

In the resting enzyme, only one strong propionate bending vibration is observed at 378 cm^{-1}. The binding of substrate analogues enhances a second propionate bending vibration at lower frequency (368 cm^{-1}), while the frequency of the original vibration remains unchanged but with a reduced intensity. The presence of two bending modes indicates the distinct conformation of the two propionate groups. It has been reported that the frequency of the propionate bending mode relates to the hydrogen-bonding network between the propionate groups and the amino acid residues (*29*). As seen in deoxy-hemoglobin (Hb) *I* (*29*), Mb (*30*), Hb A and Hb M Iwate (*31*, *32*), and P450 (*33*), disruption of the hydrogen-bonding network lowers the frequency of the propionate bending mode by about 10 cm^{-1}. It was proposed that hydrogen bonds to well-ordered amino acid residues will be more likely to restrict the motion of the propionate than

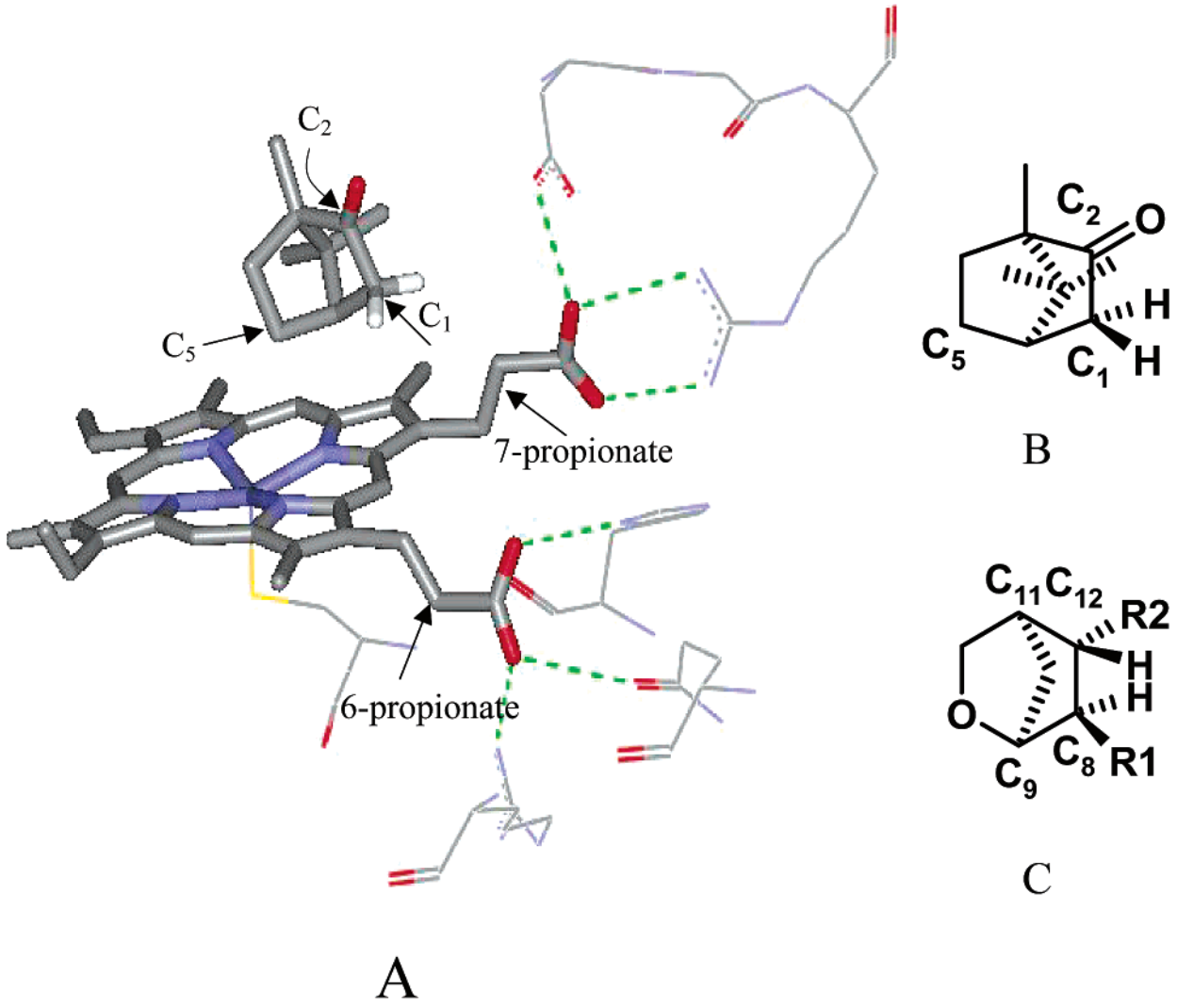

FIGURE 9: (A) Protein environment around the heme propionate groups of $P450_{cam}$ (PDB 2CPP). (B) Structure of camphor. (C) Structure of substrate analogue U44069, R_1=$CH_2CHCH(CH_2)_3CO_2H$, and R_2=$CHCHCH(OH)(CH_2)_4CH_3$.

hydrogen bonds to the more disordered bulk solvent molecules (*33*). According to these studies, the new vibrational mode at 368 cm^{-1} appearing on the introduction of substrate analogues into the heme pocket of TXAS suggests the disruption of the hydrogen-bonding network of one of the propionate groups. Unfortunately, it is currently not possible to indicate which propionate, either the 6- or the 7-propionate, is affected. The crystal structure of camphor bound P450cam, however, can provide a structural basis. In this crystal structure, the camphor molecule sits inside the distal heme pocket with its C(5) facing the heme iron, while C(1) and C(2) are the closest carbons with respect to the two propionate groups, as shown in Figure 9. The distance from these two carbons to the carboxylate groups of the heme propionates is 6−8 Å. When the picture for the camphor bound P450 is valid for TXAS, the O(9) oxygen atom in U44069 (corresponding to the C(5) carbon in camphor) will coordinate to the heme iron, which has been indicated by previous EPR and absorption experiments and resonance Raman data in this paper. The long side chain (about 9 Å) protruding from C(8) of U44069 (corresponding to C(1) in camphor) would lie above the pyrrole ring bearing the 6-propionate group, with its carboxylate oxygen at the end interfering with the 6-propionate hydrogen-bonding network.

This proposed side-chain-disruption model is further supported by our experiments on imidazole, miconazole, and U46619 bound TXAS and by site-directed mutation experiments (*42*). As shown in Figure 4, line d, the propionate bending vibration pattern does not change upon binding of imidazole. This result can be appreciated since imidazole has no side chain that can disrupt the propionate hydrogen-bonding network. The side chain of miconazole is as long as 9 Å, and in this case, two propionate bending modes are observed, indicating that miconazole can interact with one of the propionate groups and disrupt its hydrogen-bonding network. According to previous results with mutants of TXAS, the 6-propionate is hydrogen bonded to two amino acid residues, Trp-133 and Arg-137 (*42*). Mutations of these two amino acid residues lead to the loss of heme content and lower the affinity for the substrate analogue U44069. The interaction between U44069 and Arg137 is obvious in the substitution of Arg137 for lysine, in which the enzyme has a greatly decreased affinity for this substrate analogue, while the heme content does not change much. We propose that the substrate analogues, especially U44069, interact with Arg137, disrupting the hydrogen-bonding between 6-propionate and Arg137, which leads to a change of the 6-propionate bending mode from 378 to 368 cm^{-1}. This also

suggests that a similar interaction occurs when substrate PGH_2 binds in the TXAS heme pocket.

U46619 induces a distinct perturbation of the propionate bending modes from U44069. A strong propionate bending mode occurs at lower frequency, 368 cm^{-1}, on addition of substrate analogue U44069, while on binding of U46619 this vibrational mode appears as a weak shoulder very similar to miconazole, Figure 4. As explained in the binding model, the O(9) of U44069 coordinates with the heme iron, with its long carboxylate side chain disrupting the hydrogen bonding of the 6-propionate group, resulting in a lower frequency of the propionate bending mode. Presumably, this interaction involves the amino acid residue R137, which forms hydrogen bonds with the 6-propinate group based on an earlier study (*42*). When substrate analogue U46619 was introduced into the heme pocket, its O(11) can coordinate to the heme iron, but it is unlikely that its carboxylate side chain can compete for the hydrogen bonding of the propionate group as effective as that of U44069 because of a different orientation of its carboxylate group with respect to the heme iron. Its two bulky side chains, however, can cause changes in the protein matrix, as happens in the miconazole-bound enzyme, disrupting the hydrogen bonding network of propionate groups, leading to a propionate bending mode at 368 cm^{-1}, with reduced intensity. The low-frequency spectra of TXAS-U46619 and TXAS-miconazole are very similar, suggesting similar interaction of these ligands with the propionate groups. Experiments on mutant TXAS are planned to corroborate our proposal.

The vinyl vibrational pattern also illustrates the heme−protein interaction. It has been reported that vinyl groups of heme have two stable conformations (*34*−*39*): one is an in-plane conformation (relative to the heme plane) in which the vinyl groups conjugates with the heme, and the stretching vibration is detected at 1620 cm^{-1}, and the other is an out-of-plane conformation, which has a higher stretching frequency than the in-plane conformer, detected at 1631 cm^{-1}. For the bending mode, no calculation has been done, but based on isotopic labeling experiments, the bending mode with the higher frequency in Mb was assigned to the 2-vinyl group, while the lower frequency mode was assigned to the 4-vinyl group (*27*). As indicated in crystal structures of Mb, the 2-vinyl group has a torsion angel that is 40−50° larger than that of the 4-vinyl group (measured from PDB entries 1YMB and 1WLA). In light of these observations, we assign the vibrations at 1630 and 424 cm^{-1} in TXAS to the stretching and bending vibrations of the out-of-plane vinyl group, respectively, while the vibrations at 1621 and 408 cm^{-1} are those of the in-plane conformer.

Most of the previous studies have focused on the stretching modes, but the bending vibrations reported here show more clearly the heme−protein interaction. For the resting enzyme, the vinyl bending vibration at 408 cm^{-1} is much stronger than at 424 cm^{-1} (Figure 4, line a), indicating that the in-plane conformer is dominant over the out-of-plane conformer. Introduction of ligands into the heme pocket greatly enhances the vibration at 424 cm^{-1}, while the vibration at 408 cm^{-1} is reduced in its intensity (Figure 4, lines b−e), suggesting that the population of out-of-plane conformer increases. Studies on model compounds (*34*), indoleamine 2,3-dixoygenase [IDO] (*35*), peroxidases (*36*−*38*), and KatG (*39*) have implied that restriction enforced by the protein matrix forces both of the two vinyl groups into an in-plane conformation, while introducing ligands into the heme pocket or mutation of some amino acids causes rearrangement of the protein environment and increases the population of the out-of-plane conformer. The present data suggests this kind of protein environment rearrangement occurs to accommodate the ligands when they bind to the heme iron of TXAS and that one of the vinyl groups is forced to out of the heme plane.

Comparison of TXAS to P450, CPO, and NOS. The detection of the Fe−S vibration at 350 cm^{-1} confirms the characterization of TXAS as a cytochrome P450 type enzyme, which is designated as a group of hemoproteins with a cysteine thiolate ligand at the proximal coordination site of the heme iron. The Fe−S stretching vibration measured for TXAS is close to that of P450 and CPO, which are detected at 351 and 347 cm^{-1}, respectively, and higher than that of NOS at 338 cm^{-1} (*12*, *15*, *20*). A correlation between the basicity of the proximal ligand and the stretching frequency has been observed: the higher the basicity of the proximal ligand, the higher the stretching frequency (*43*). Furthermore, the reactivity of heme Fe with respect to oxygen shows a correlation with νFe−His (*44*). Comparison of the Fe−S vibrational frequencies observed in various hemethiolate enzymes indicates that the basicity of the cysteine thiolate in TXAS is similar to that in P450 and CPO and higher than that in NOS. The basicity of cysteine thiolate was proposed to depend on the hydrogen bond formation to the cysteine ligand and heme plane distortion (*20*). In P450 and CPO, the proximal thiolate hydrogen bonds to two peptide NH groups (*45*−*47*). In NOS, the proximal thiolate accepts a hydrogen bond from a peptide NH group and an indole nitrogen proton of a Trp residue, and the heme plane was found to more distorted than that in P450 (*48*, *49*). The strength of Fe−S bond, as determined by the Fe−S vibrational frequency, suggests that the heme geometry and hydrogen bonding to the proximal thiolate in TXAS are similar to those of P450 and CPO, and we propose that two hydrogen bonds from peptide NH group connect to the cysteine thiolate group in TXAS and that the heme plane in TXAS is less distorted than in NOS.

It is believed that the proximal cysteine thiolate ligand plays a critical role in the catalytic cycle of cytochrome P450 enzymes (*10*, *11*, *50*−*52*). From DFT calculations, a sulfur radical has been predicted to be an alternative formulation of the intermediate, compound I, instead of a porphyrin radical cation (*11*). Since the Fe−S stretching frequency is similar, the electron density between the Cys-S and the Fe atom is expected to be very close between TXAS and P450/CPO. This suggests that the reactivity of the proximal ligand and the heme iron with respect to substrate is also similar in TXAS as compared to P450 and CPO. This result is rather surprising, given the different chemistry that is catalyzed in these enzymes. Experiments to detect the reaction intermediates are underway in our laboratory.

CONCLUSIONS

We report the first resonance Raman characterization of TXAS in both the absence and the presence of substrate analogues. The observation of a 6c/ls heme in U46619-bound TXAS contradicts an earlier result based on optical difference

spectroscopy. The new evidence reported here indicates that both the O(9) and the O(11) of the substrate can coordinate to the heme iron of TXAS, which suggests that the reaction of TXAS with PGH_2 may also occur with O(11) coordinated to the heme iron, which may lead to a side reaction resulting in inhibition of the enzyme, or perhaps, formation of MDA and HHT.

The bending modes of the vinyl and propionate groups detected in the resting and substrate analogue bound TXAS indicate that the vinyl groups predominately assume the in-plane conformation for the resting enzyme and that the propionate groups form a strong hydrogen-bonding network with some amino acid residues. On addition of substrate analogues, and presumably PGH_2, the carboxylate group side chain disrupts the hydrogen-bonding network of one of the propionate groups, most likely the 6-propionate group. At the same time, the substrate causes the protein environment to rearrange, and one of the vinyl groups is forced out of the heme plane.

We have also measured the Fe−S stretching frequency at 350 cm^{-1} in the 5c/hs form of TXAS with CTA_2 bound. The frequency of this vibration is close to those of P450 and CPO and higher than in NOS. Therefore, the strength, as well as the electron density, of the Fe−S bond in TXAS is similar as in P450 and CPO. Since this bond is believed to be critically involved in the formation of reaction intermediates in the catalytic cycles of P450 and CPO, the similar Fe−S bond suggests that the chemical reactivity of the heme iron in TXAS resembles that in P450 and CPO.

ACKNOWLEDGMENT

We acknowledge Ms. Pei-Yung Hsu for her technical assistance.

REFERENCES

1. Samuelesson, B., Golddyn, M., Granstrom, E., and Malmsten, C. (1978) *Annu. Rev. Biochem. 47*, 997−1029.
2. Ogletree, M. L. (1987) *Fed. Proc. 46*, 133−138.
3. Ullrich, V., Zou, M. H., and Bachschmid, M. (2001) *Biochim. Biophys. Acta 1532*, 1−14.
4. Haurand, M., Ullrich, V. (1985) *J. Biol. Chem. 261*, 15059−15067.
5. Ohashi, K., Ruan, K. H., Kulmacz, R. J., Wu, K. K., and Wang, L. H. (1992) *J. Biol. Chem. 267*, 789−793
6. Hsu, P. Y., Tsai, A. L., Kulmacz, R. J., and Wang, L. H. (1999) *J. Biol. Chem. 274*, 762−769.
7. Sligar, S. C. (1999) *Essays Biochem. 34*, 71−83
8. Hecker, M., Ullrich, V. (1989) *J. Biol. Chem. 264*, 141−150.
9. Ullrich, V., and Brugger, R. (1994) *Angew. Chem., Int. Ed. Engl. 33*, 1911−1919.
10. Green, M. T. (1998) *J. Am. Chem. Soc. 120*, 10772−10773.
11. Green, M. T. (1999) *J. Am. Chem. Soc. 121*, 7939−7940.
12. Champion, P. M., Stallard, B. R., Wagner, G. C., and Gunsalus, I. G. (1982) *J. Am. Chem. Soc. 1104*, 5469−5472.
13. Wells, A. V., Li, P., and Champion, P. M. (1992) *Biochemistry 31*, 4383−4393.
14. Bangcharoenpaurpong, O., Champion, P. M., Martinis, S. A., and Sligar, S. G. (1987) *J. Chem. Phys. 87*, 4273−4284.
15. Bangcharoenpaurpong, O., Hall, K. S., Hager, L. P., and Champion, P. M., (1986) *Biochemistry 25*, 2374−2378.
16. Green, E. L., Taoka, S., Banerjee, R., and Loehr, T. M. (2001) *Biochemistry 40*, 459−463.
17. Wang, J. L., Stuehr, D. J., Ikeda, M., and Rousseau, D. L. (1993) *J. Biol. Chem. 268*, 22255−22258.
18. Rodriguez-Crespo, I., Moenne-Loccoz, P., Loehr, T., and Montellano, P. R. O. (1997) *Biochemistry 36*, 8530−8538.
19. Couture, M., Stuehr, D. J., and Rousseau, D. L. (2000) *J. Biol. Chem. 275*, 3201−3205.
20. Schelvis, J. P. M., Berka, V., Babcock, G. T., and Tsai, A. L. (2002) *Biochemistry 41*, 5695−5701.
21. Wang, L.-H., Tsai, A.-L., and Hsu, P.-Y. (2001) *J. Biol. Chem. 276*, 14737−14743.
22. Abe, M., Kitagawa, T., and Kyogoku, Y. (1978) *J. Chem. Phys. 69*, 4526−4534.
23. Choi, S., and Spiro, T. G. (1983) *J. Am. Chem. Soc. 105*, 3683−3692.
24. Choi, S., Lee, J. J., Wei, Y. H., and Spiro, T. G. (1983) *J. Am. Chem. Soc. 105*, 3692−3707.
25. Vickery, L. E. (1991) *Methods Enzymol. 206*, 548−558.
26. Evangalista-Kirkup, R., Crisanti, M., Poulos, T. L., and Spiro, T. G. (1985) *FEBS Lett. 190*, 221−226.
27. Hu, S., Smith, K. M., and Spiro, T. G. (1996) *J. Am. Chem. Soc. 118*, 12638−12646.
28. Hu, S., Morris, I. K., Singh, J. P., Smith, K. M., and Spiro, T. G. (1993) *J. Am. Chem. Soc. 115*, 12446−12458.
29. Cerda-Colon, J. F., Silfa, E., and Lopez-Garriga, J. (1998) *J. Am. Chem. Soc. 120*, 9312−9317.
30. Peterson, E. S., Friedman, J. M., Chien, E. Y. T., and Sligar, S. G. (1998) *Biochemistry 37*, 12301−12319.
31. Nagai, M., Aki, M., Jin, Y., Sakai, H., Nagatomo, S., and Kitagawa, T. (2000) *Biochemistry 39*, 13093−13105.
32. Hildebrandt, P., Burk, D. L., Maurus, R., Ferrer, J. C., Brayer, G. D., and Mauk, A. G. (1995) *Biochemistry 34*, 1997−2005.
33. Hildebrandt, P., Heibel, G., Anzenbacher, P., Lange, R., Kruger, V., and Stier, A. (1994) *Biochemistry 33*, 12920−12929.
34. Kalsbeck, W. A., Ghosh, A., Pandey, R. K., Smith, K. M., and Bocian, D. F., (1995) *J. Am. Chem. Soc. 117*, 10959−10968.
35. Terebtis, A. C., Thmos, S. R., Takikawa, O., Littlejohn, T. K., Truscott, R. J. W., Armstrong, R. S., Yeh, S. R., and Stocker, R. (2002) *J. Biol. Chem. 277*, 15788−15794.
36. Neri, F., Indiani, C., Baldi, B., Vind, J., Welinder, K. G., and Smulevich, G. (1999) *Biochemistry 38*, 7819−7827.
37. Nissum, M., Neri, F., Mandelman, D., Poulos, T. L., and Smulevich, G. (1998) *Biochemistry 37*, 8080−8087.
38. Neri, F., Kok, D., Miller, M. A., and Smulevich, G. (1997) *Biochemistry 36*, 8947−8953.
39. Lukat-Rodgers, G. S., Wengenack, N. L., Rusnak, F., and Rodgers, K. R. (2000) *Biochemistry 39*, 9984−9993.
40. Chen, P. F., Berka, V., Tsai, A. L., and Wu, K. K. (1998) *J. Biol. Chem. 273*, 3464−3470
41. Hecher, M., Baader, W. J., Weber, P., and Ullrich, V. (1987) *Eur. J. Biochem. 169*, 563−569.
42. Hsu, P. Y., Tsai, A. L., and Wang, L. H. (2000) *Arch. Biochem. Biophys. 383*, 119−127.
43. Teraoka, J., and Kitagawa, T. (1981) *J. Biol. Chem. 256*, 3969−3977.
44. Oertling, W. A., Kean, R. T., Wever, R., and Babcock, G. T. (1990) *Inorg. Chem. 29*, 2633−2645.
45. Poulos, T. L., Finzel, B. C., Gunsalus, I. C., Wagner, G. C., and Kraut, J. (1985) *J. Biol. Chem. 260*, 16122−16130.
46. Schlichting, I., Berendzen, J., Chu, K., Stock, A. M., Maves, S. A., Benson, D. E., Sweet, R. M., Ringe, D., Petsko, G. A., and Sligar, S. G. (2000) *Science 287*, 1615−1622.
47. Sundaramoonrthy, M., Terner, J., and Poulos, T. L. (1995) *Structure 3*, 1367−1377.
48. Raman, C. S., Li, H., Martasek, K., Kral, V., Master, B. S., and Poulos, T. L. (1998) *Cell 95*, 939−950.
49. Crane, B. R., Arvai, A. S., Gachhui, R., Wu, C., Ghosh, D. K., Getzoff, E. D., Stuehr, D. J., and Tainer, J. A. (1997) *Science 278*, 425−431.
50. Sono, M., Roach, M. P., Coulter, E. D., and Dawson, J. H. (1996) *Chem. Rev. 96*, 2841−2887.
51. Daiber, A., Nauser, T., Nakaya, N., Kudo, T., Weber, P., Hultschig, C., Shoun, H., Ullrich, V. (2002) *J. Inorg. Biochem. 88*, 343−352.
52. Visser, S. P., Ogliaro, F., Sharma, P. K., and Shaik, S. (2002) *J. Am. Chem. Soc. 124*, 11890−11826.

BI027206S